Heliyon 10 (2024) e29386

Contents lists available at ScienceDirect

Heliyon

journal homepage: www.cell.com/heliyon

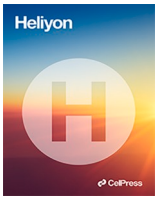

Research article

KIF15 promotes the development and progression of chordoma via activating PI3K-AKT signalling pathway

Jinxing Yang, Lijun Liu, Xu Xu, Hui Zeng *

First Affiliated Hospital of Shenzhen University/Shenzhen Second People's Hospital, Shenzhen, Guangdong, 518000, China

ARTICLE INFO

Keywords:
Chordomas
KIF15
PI3K-AKT pathway

ABSTRACT

Aims: Despite its implication in various human cancers, the expression and functional significance of Kinesin family member 15 (KIF15) in chordomas remain unexplored.
Main methods: The evaluation of KIF15 protein levels was conducted through immunohistochemistry (IHC) staining and Western blot analysis. Cell proliferation was quantified using MTT and CCK8 assays, whereas cell migration was examined using wound healing and Transwell assays. Furthermore, flow cytometric analysis was utilized to assess cell apoptosis and the cell cycle. Additionally, *in vivo* experiments were performed using a mouse xenograft model.
Key findings: Our study revealed significantly higher expression of KIF15 in stage III chordoma tissues compared to stage II tissues. Knockdown of KIF15 led to notable inhibition of cell proliferation and migration, along with enhanced apoptosis and cell cycle arrest. *In vivo* studies further confirmed the inhibitory effects of KIF15 knockdown on chordoma tumour growth. In terms of mechanism, we identified the involvement of the PI3K-AKT signalling pathway mediated by KIF15 in chordomas. Notably, the anti-tumour effects of KIF15 deficiency on chordomas were partially reversed by the addition of an AKT activator.
Significance: KIF15 promotes chordoma development and progression through the activation of the PI3K-AKT signalling pathway. Thus, targeting KIF15 might be a promising therapeutic strategy for treating chordomas.

1. Introduction

Chordomas, constituting approximately 9.8 % of malignant bone tumours, are low-grade malignant tumours originating from residual notochord tissues in embryos [1–3]. Owing to their local invasiveness and resistance to conventional chemotherapy, the preferred treatment approach involves surgical resection coupled with adjuvant radiotherapy [4,5]. Despite this strategy, patients often encounter recurrence and experience poor prognosis postoperatively, presenting a considerable challenge in the management of chordomas [5]. Recent advancements in the study of chordomas have provided profound understanding of the underlying molecular mechanisms, including the involvement of specific molecules, signalling pathways, and microRNAs. This enhanced comprehension has fuelled progress in the development of targeted therapeutic strategies for chordoma treatment [6,7]. Illustrative examples include imatinib, nilotinib, and sunitinib, which have exhibited therapeutic efficacy by specifically targeting the platelet-derived growth factor receptors-α and β [8–10]. However, due to the limited understanding of chordoma pathogenesis, the effectiveness of these targeted

* Corresponding author. First Affiliated Hospital of Shenzhen University/Shenzhen Second People's Hospital, No.3002, Sungang West Road, Shenzhen, 518000, China.
E-mail address: zenghui@pkuszh.com (H. Zeng).

https://doi.org/10.1016/j.heliyon.2024.e29386
Received 14 June 2023; Received in revised form 7 April 2024; Accepted 7 April 2024
Available online 9 April 2024

inhibitors has been constrained [11]. Therefore, identifying additional crucial targets will not only enhance our understanding of the pathogenesis of chordoma, but also establish a robust foundation for developing new targeted drugs, ultimately improving the efficacy of chordoma treatment.

Kinesin family member 15 (KIF15), also referred to as Kinesin-12, is a microtubule-dependent kinesin crucial for mitosis and bipolar spindle assembly, often collaborating with eg5 [12]. Previous studies have consistently linked KIF15 to the development and progression of various human cancers, suggesting its potential as a target for anticancer therapies [13]. Subsequent studies identified KIF15's involvement in specific cancer types, such as its role as a promoter in prostate cancer [14] and its contribution to the proliferation of bladder and pancreatic cancer cells through the MEK/ERK signalling pathway [15,16]. Investigations by Gao et al. suggested KIF15's regulatory effects on breast cancer cell phenotypes, including proliferation and migration [17]. Furthermore, the effectiveness of KIF15 inhibition, notably with KIF15-IN-1, has been documented in impairing cancer cell growth [18]. Despite extensive research across different cancer types, the precise role of KIF15 in chordoma pathogenesis remains elusive and unexplored. Therefore, it is imperative to investigate KIF15's potential as a therapeutic target in chordomas to advance our understanding and potentially enhance treatment approaches.

Our investigation revealed elevated KIF15 expression in human chordoma tissues and cells. Notably, suppressing KIF15 markedly retarded chordoma progression by regulating the PI3K-AKT signalling cascade. These results highlight the promising potential of KIF15 as a therapeutic target for chordoma management.

2. Materials and methods

2.1. Collection of clinical samples

We obtained a human chordoma tissue microarray consisting of 24 paraffin-embedded specimens from Xi'an Alina Biological Technology Co., Ltd. Prior to tissue collection, written informed consent was obtained from all patients. The study protocol received approval from the Medical Ethics Committee of Guangdong Provincial People's Hospital.

2.2. Cell lines and cell culture

Human Embryonic Kidney 293T (HEK-293T) cells, MUG-Chor1, and U–CH1 chordoma cell lines were procured from American Type Culture Collection (ATCC, Cat. #CRL-3216 for HEK-293T cells, Cat. #CRL-3219 for MUG-Chor1 cells and Cat. #CRL-3217 for U–CH1 cells). HEK-293T cells were cultured in RPMI-1640 medium supplemented with 10 % FBS and 1 % penicillin/streptomycin, while chordoma cell lines were cultured in the same medium but without the addition of penicillin/streptomycin. All cells were maintained at 37 °C with 5 % CO_2, following ethical guidelines and obtaining written informed consent. Additionally, rigorous measures were taken to ensure that the cells used in the experiments were free from mycoplasma contamination. Cell line authentication was performed via Short Tandem Repeat (STR) analysis at the beginning of the experiment. Genomic DNA from each cell line was subjected to PCR amplification using multiple universal fluorescent primers, and the resulting pattern was compared to a reference pattern, verifying the authenticity of each cell line. As a routine practice, we periodically re-authenticate our cell lines every four months, both prior to cryopreservation and following the initial week of cell culture. The most recent authentication testing was conducted in December 2023.

2.3. Immunohistochemistry (IHC) staining

De-paraffinized sections of human chordoma tissues underwent antigen retrieval using 1 × EDTA (Beyotime Biotechnology Co., Ltd., Shanghai, China) and were then treated with 3 % H_2O_2 for 5 min to block endogenous peroxidase activity. Following this, the sections were incubated overnight at 4 °C with primary antibodies, specifically KIF15 (1:100, fine test) or Ki-67 (1:300, Abcam), followed by 1-h incubation at 37 °C with the secondary antibody (goat anti-rabbit IgG H&L (HRP):1:400, Abcam, Cambridge, MA, USA). Visualization was achieved using DAB for 5 min and hematoxylin for 15 s (Baso Diagnostics Inc., Zhuhai, China). The slides were sealed with neutral resin (China National Pharmaceutical Group Co., Ltd., Beijing, China) before capturing images and subsequent analysis under an optical microscope. Three independent pathologists conducted image analysis to evaluate staining patterns and assigned scores based on staining percentage (1–24 %: 1, 25–49 %: 2, 50–74 %: 3, 75–100 %: 4) and intensity (0: no signal, 1: light yellow, 2: brown-yellow, 3: dark brown). The median IHC scores across all tissues were used to delineate parameters for high and moderate expression levels.

2.4. Overexpression plasmids and lentivirus RNAi construction and transfection

Three knockdown sequences targeting KIF15, namely shKIF15-1 (GCTGAAGTGAAGAGGCTCAAA), shKIF15-2 (AGGCAGCTAGAATTGGAATCA), and shKIF15-3 (AAGCTCAGAAAGAGCCATGTT), were designed based on the KIF15 gene template by Shanghai Yibeirui Biomedical Science and Technology Co., Ltd. The BR-V-108 vector was sourced from the same biomedical company in Shanghai, China. For cell transfection, a negative control (shCtrl) utilizing an RNAi scramble sequence (TTCTCCGAACGTGTCACGT) was employed. The interference sequences were synthesized into single-stranded DNA oligos, annealed, and paired to form double-stranded DNA. Subsequently, double-stranded DNA was directly ligated to the BR-V-108 vector through the restriction sites present at both ends, maintained at 16 °C for 1 h. This ligation product was then transformed into the prepared TOP 10 E. coli competent cells

(TIANGEN, Cat. #CB104-03) while keeping them on ice for 30 min. Additionally, a lentiviral vector overexpressing KIF15 was constructed, utilizing the primer amplification sequence specific to KIF15. Positive recombinants were identified using qPCR and confirmed by sequencing. Lentivirus transfection into MUG-Chor1 and U–CH1 cells was conducted. LipofectamineTM 3000 Transfection Reagent (Thermofisher, Cat. #L3000015) was utilized as the transfection agent. Transfection efficiency was determined by quantifying transfected cells expressing green fluorescent protein (GFP). Specifically, fluorescence microscopy was employed to analyze and quantify GFP-expressing cells in shKIF15-1-transfected cells. The percentage of GFP-positive cells in the total cell population was calculated, yielding the 80 % transfection efficiency as successful.

2.5. RNA extraction, cDNA synthesis, and quantitative reverse transcription-polymerase chain reaction (qRT-PCR)

Total RNA was isolated utilizing TRIzol reagent (Sigma-Aldrich), followed by cDNA synthesis and qRT-PCR using the Promega M-MLV Kit (Promega Corporation, Madison, Wisconsin, USA) and SYBR Green Master Mix Kit (Vazyme, Nanjing, Jiangsu, China), respectively. GAPDH served as the internal control. mRNA expression was relatively quantified using the $2^{-\triangle\triangle Ct}$ method. The primer sequences (5′–3′) were as follows: KIF15: CTCTCACAGTTGAATGTCCTTG (forward) and CTCCTTGTCAGCAGAATGAAG (reverse); GAPDH: TGACTTCAACAGCGACACCCA (forward) and CACCCTGTTGCTGTAGCCAAA (reverse).

2.6. Western blot assay

Proteins were isolated and subjected to 10 % sodium dodecyl sulphate-polyacrylamide gel electrophoresis (SDS-PAGE), followed by Western blot. PVDF membranes were blocked in TBST solution with 5 % skim milk for 1 h at room temperature. After blocking, the membranes were probed with primary antibodies at room temperature for 2 h, which included KIF15 (1:2000, fine test, # FNab04551), AKT (1:2000, Proteintech, # 10176-2-AP), *p*-AKT (1:2000, Proteintech, # 66444-1-Ig), PI3K (1:2000, Proteintech, # 67071-1-Ig), p-PI3K (1:500, Bioss, bs-3332R) and GAPDH (1:3000, Bioworld, # AP0063). Following primary antibody incubation, membranes were exposed to Goat Anti-Rabbit (1:3000, Beyotime, # A0208) and Goat Anti-Mouse (1:3000, Beyotime, # A0216) secondary antibodies for 1 h at room temperature. After a series of washes with blocking solution, colorimetric detection was carried out using the ECL + plusTM western blotting system.

2.7. Cell proliferation detection

Cell proliferation was assessed through two methods. Firstly, the MTT experiment involved seeding MUG-Chor1 and U–CH1 cells, transfected with shCtrl and shKIF15, in 96-well plates. After incubation, MTT solution was added, followed by DMSO, and OD was measured at 490 nm over 5 days.

The second method, the CCK8 assay, included treating cells with 10 μM AKT activator, 40 μM LY294002 (PI3K inhibitor), or 10 μM GW406108X (KIF15 inhibitor) for 24 h. Following treatment, 10 μL of CCK-8 reagent was added, and the optical density (OD) was measured at 450 nm after 24–48 h of incubation. Each experimental was repeated thrice, and statistical analyses were conducted for interpretation.

2.8. Wound healing assay

Chordoma cells, treated with either shCtrl or shKIF15, were trypsinised to generate a cell suspension. The cells were then seeded into a 96-well plate at a density of 3.5×10^4 cells/well, ensuring a cell confluence of over 90 %. Each experimental group had three duplicate wells, and the culture volume per well was maintained at 100 μL. The following day, a low-concentration serum medium was added, and a scratch was made at the center of the lower end of the plate to create wounds in the cell monolayer. Next, the cells underwent a wash with a serum-free medium before adding 0.5 % FBS. Subsequently, the cells were placed in a controlled environment with 5 % CO_2 at 37 °C for incubation. To assess the healing progress, the plates were scanned at 24 and 48 h, and the migration area was quantitatively analyzed using Cellomics software.

2.9. Transwell assay

Chambers were set in a 24-well plate and left to incubate for 2 h. Initially, each chamber received 100 μL of serum-free medium, which was then removed after 1–2 h. In parallel, the lower chambers were supplemented with 600 μL of a medium enriched with 30 % FBS. Following this, MUG-Chor1 and U–CH1 cells transfected with either shKIF15 or shCtrl were prepared in a cell suspension using a low serum concentration and seeded in the upper chambers at a density of 1×10^5 cells/mL. These chambers were then placed into the lower chamber and allowed to incubate for 24 h. After incubation, to facilitate staining, 400 μL of a staining solution was introduced into the vacant wells of a 24-well plate, where the chambers were submerged for 5 min. The capability of the cells to migrate was evaluated based on data collected from three independent experiments.

2.10. Detection of cell apoptosis and cell cycle by fluorescence activated cells sorting (FACS)

MUG-Chor1 and U–CH1 cells, post-lentiviral transfection, were cultured in 6-well plates until reaching 85 % confluence. After centrifugation at 1300 *g*, the supernatant was carefully removed, and cells were washed with4°C D-Hanks (pH = 7.2–7.4). Staining

with 10 μL Annexin V-APC (eBioscience, San Diego, CA, USA) was conducted for 10 min in the dark to evaluate cell apoptosis using a FACSCalibur (BD Biosciences, San Jose, CA, USA). For double-staining experiment, 5 μL of Annexin V-APC and 5 μL of propidium iodide (PI) solution were sequentially added, followed by FACSCalibur detection.

For cell cycle analysis, a 5 mL/well cell suspension was cultured in 6-cm dishes until reaching 70 % confluence. After centrifugation at 1200 *g* for 5 min, cells were washed with 4 °C PBS and ethanol, then stained with PI solution. Changes in the cell cycle were assessed using FACSCalibur (BD Biosciences, San Jose, CA, USA).

2.11. Construction of nude mouse tumour formation model

Male BALB/c nude mice aged four weeks were procured from Beijing Weitong Lihua Technology Co., Ltd., and evenly allocated into two groups, each comprising 10 mice. Ethical clearance for the animal experimentation was secured from the Medical Ethics Committee of Guangdong Provincial People's Hospital. Xenograft models were induced by subcutaneously injecting MUG-Chor1 cells transfected with either shCtrl or shKIF15, with a dose of 4×10^6 cells per mouse. Tumour dimensions were monitored using Vernier calipers for an 18-day duration. At the study's conclusion, mice were euthanized with 0.7 % sodium pentobarbital (10 μL/g) administered intraperitoneally, and fluorescence was assessed employing the *in vivo* imaging system (IVIS Spectrum, PerkinElmer). Following sacrifice, tumours were excised, weighed, and promptly cryopreserved in liquid nitrogen at −80 °C.

2.12. PrimeView human gene expression array

The PrimeView human gene expression array was conducted on MUG-Chor1 cells transfected with shCtrl/shKIF15. RNA extraction followed established protocols, with RNA quality assessed using a Nanodrop 2000 and Agilent 2100 with an Agilent RNA 6000 Nano Kit. Affymetrix Human GeneChip PrimeView assays were conducted strictly according to the manufacturer's guidelines, and the resulting data were captured using an Affymetrix Scanner 3000. Statistical analysis employed a Welch *t*-test with Benjamini-Hochberg

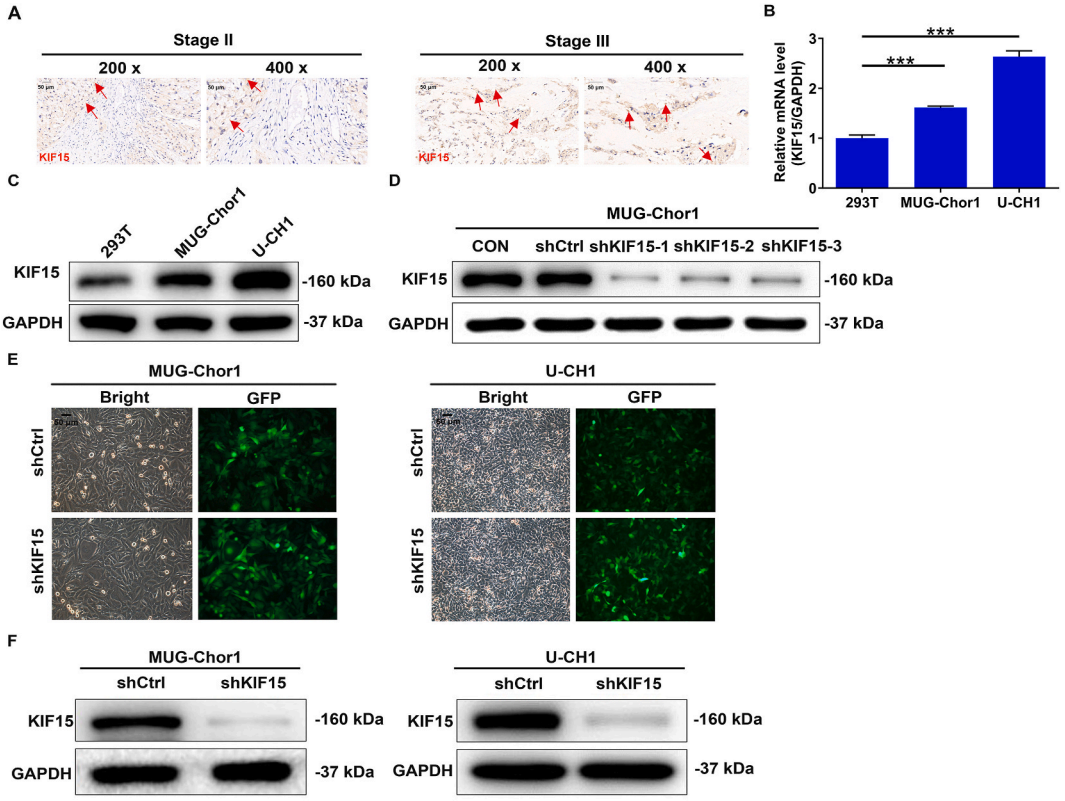

Fig. 1. KIF15 was upregulated in chordoma and KIF15 knockdown cell model was established. (A) KIF15 protein expression in chordoma tumour tissues at different pathological stages, as determined by IHC staining. Primary antibody: KIF15, Secondary antibody: goat anti-rabbit IgG H&L (HRP). Magnification times: 400 × and 200 × . Scale: 50 μm. Arrows indicate positive KIF15 staining. (B, C) The KIF15 mRNA (B) and protein (C) expression in HEK-293T cells and chordoma cell lines were analyzed by qRT-PCT and Western blot. (D) The knockdown efficiencies of KIF15 in shKIF15 group were detected by Western blot. (E) The fluorescence expression in cells was observed after 72 h-infection. Magnification times: 200 × . Scale: 50 μm. (F) The expression of KIF15 protein in chordoma cell lines after infection was detected by Western blot. Results are presented as mean ± SD.

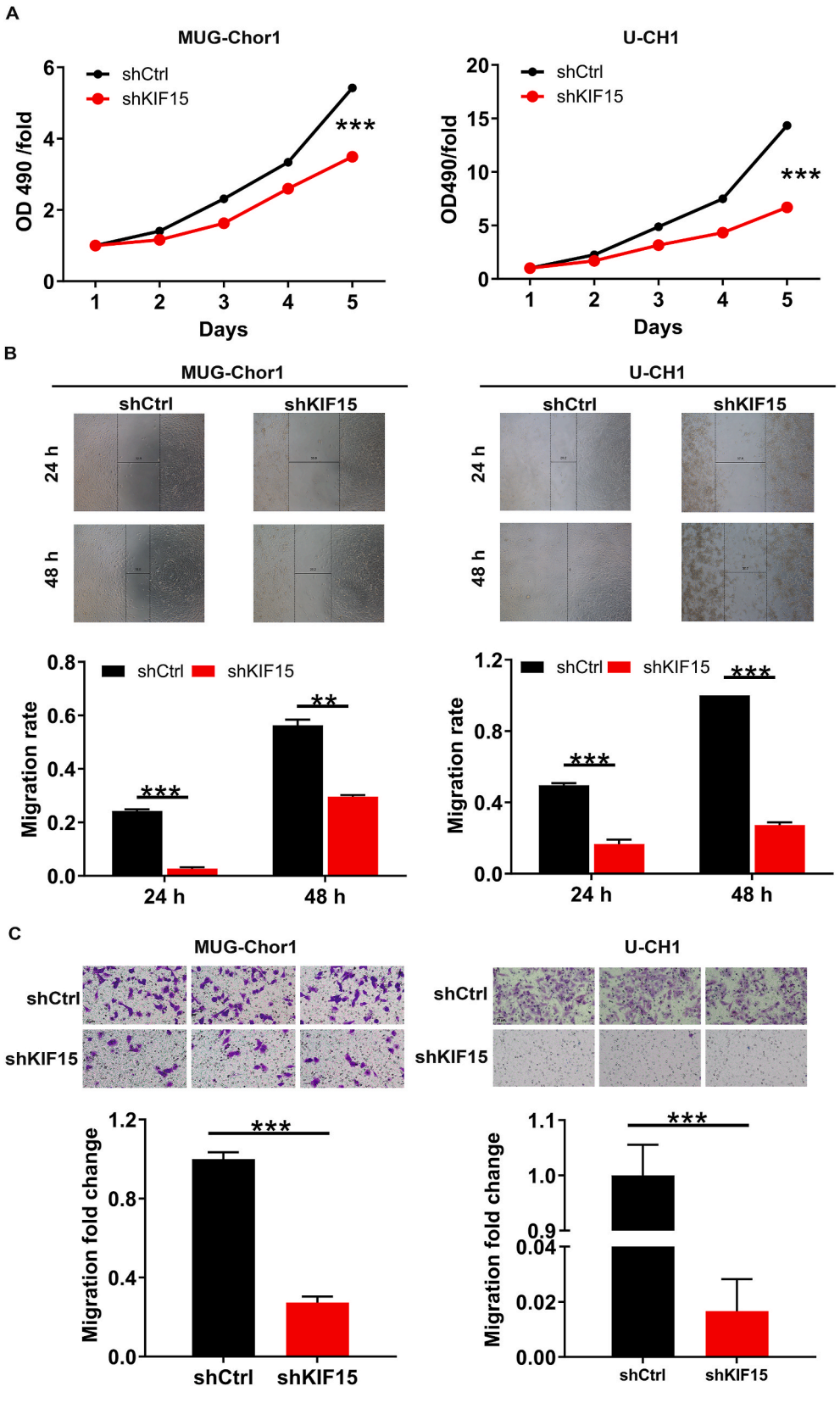

(caption on next page)

Fig. 2. KIF15 knockdown inhibited cell proliferation and migration. (A) The cell proliferation rate was evaluated in chordoma cell lines after infection by MTT assay. (B, C) The migration of chordoma cells was detected after infection by wound-healing assay (B) and transwell assay (C). Magnification times: 200 × . Scale: 50 μm. Results are presented as mean ± SD. $^{**}P < 0.01$, $^{***}P < 0.001$.

FDR, considering |Fold Change| ≥ 1.3 and FDR <0.05 as statistically significant criteria.

2.13. Statistical analysis

For data analysis, we utilized GraphPad Prism 6 software (GraphPad, San Diego, CA, USA). The data are presented as the mean ± standard deviation (SD) to reflect the variability in our measurements. Statistical significance was evaluated using the unpaired *t*-test, with a threshold of $P < 0.05$ considered significant. To ensure the reproducibility of our results, each experiment was replicated three times.

3. Results

3.1. KIF15 is abundantly expressed in chordoma

To investigate KIF15's involvement in chordomas, its expression in human chordoma tissues across different pathological stages was examined via IHC analysis. Results showed higher KIF15 protein levels in advanced chordoma tissues compared to early-stage ones (Fig. 1A). Subsequently, the expression of KIF15 was evaluated in HEK-293T cells along with the chordoma cell lines MUG-Chor1 and U–CH1. Analysis via qRT-PCR and Western blot demonstrated increased levels of both mRNA and protein of KIF15 in MUG-Chor1 and U–CH1 cells compared to HEK-293T cells (Fig. 1B and C and S1A).

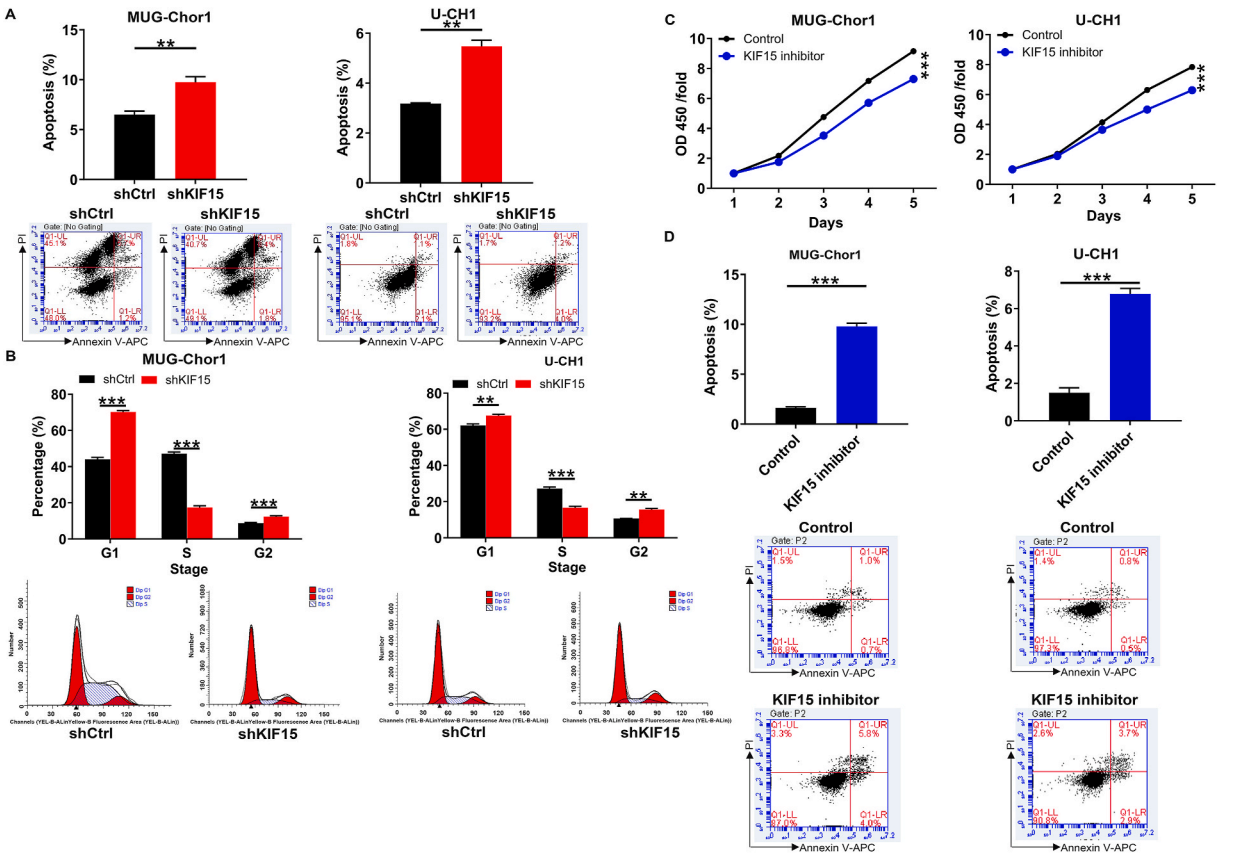

Fig. 3. The effects of KIF15 knockdown on cell apoptosis and cell cycle. (A) The effects of KIF15 knockdown on cell apoptosis were examined by flow cytometry. (B) The effects of KIF15 knockdown on cell cycle were determined by flow cytometry. (C, D) The effects of GW406108X (KIF15 Inhibitor) on cell proliferation (C) and apoptosis (D) in MUG-Chor1 and U–CH1 cells. Results are presented as mean ± SD. $^{**}P < 0.01$, $^{***}P < 0.001$.

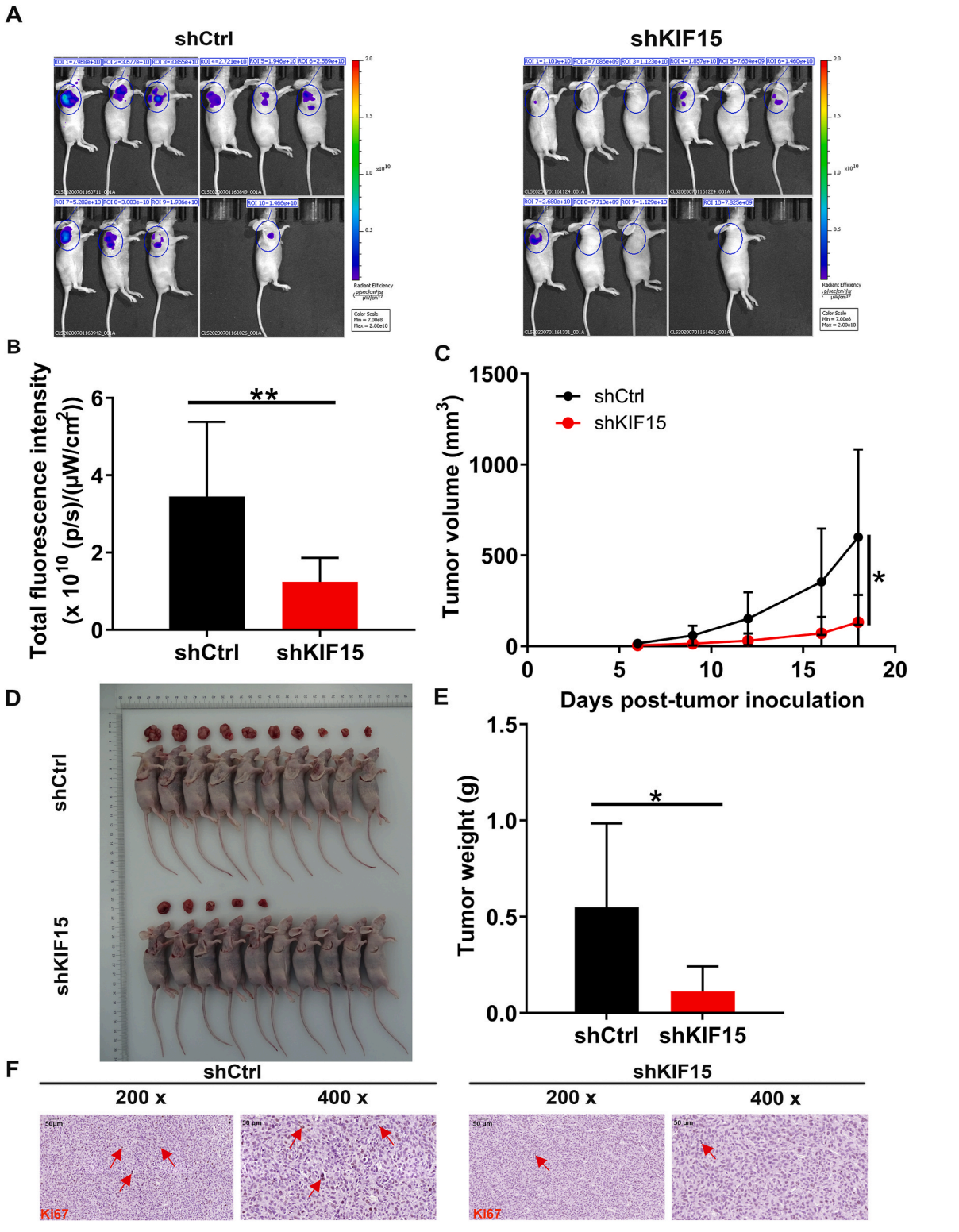

(caption on next page)

Fig. 4. KIF15 knockdown suppressed chordoma growth *in vivo*. (A) A nude mice model of KIF15 knockdown was constructed. (B) The fluorescence intensity in mouse xenograft models was tested by injecting D-Luciferase before the mice were sacrificed. (C) Tumour volume was tested from feeding to sacrifice. (D) The photograph of tumours was taken after removing tumours. (E) The tumour's weight was weighed after sacrificing mice. (F) Ki67 expression in xenograft tumours was determined by IHC staining. Primary antibody: Ki67, Secondary antibody: goat anti-rabbit IgG H&L (HRP). Magnification times: 400 × and 200 × . Scale: 50 μm. Arrows indicate positive Ki67 staining. Results are presented as mean ± SD. $*P < 0.05$, $**P < 0.01$.

3.2. Establishment of KIF15 knockdown cell models

To investigate the functional significance of KIF15 in chordomas, MUG-Chor1 cells were transfected with lentivirus plasmids shKIF15 (shKIF15-1, shKIF15-2, and shKIF15-3) to establish cell models with KIF15 knockdown. The knockdown efficiencies of shKIF15-1, shKIF15-2, and shKIF15-3 were assessed to determine the most effective lentiviral plasmid for subsequent experiments. Western blot analysis demonstrated significant downregulation of KIF15 protein levels, particularly in the shKIF15-1 group, compared to the shCtrl group (Fig. 1D and S1B). Additionally, the efficiency of shKIF15-1 transfection was evaluated by observing the GFP expression in MUG-Chor1 and U–CH1 cells, showing over 80 % transfection efficiency (Fig. 1E). Consistently, downregulation of KIF15 protein levels was confirmed in the shKIF15 groups for both cell lines (Fig. 1F and S1C). These findings confirm the successful establishment of MUG-Chor1 and U–CH1 cell models with KIF15 knockdown.

3.3. Silencing KIF15 inhibits cell proliferation and migration, induces cell apoptosis, and arrests cell cycle in vitro

In this segment, we examined the impact of KIF15 knockdown on chordoma cell behaviors. Our data revealed that silencing KIF15

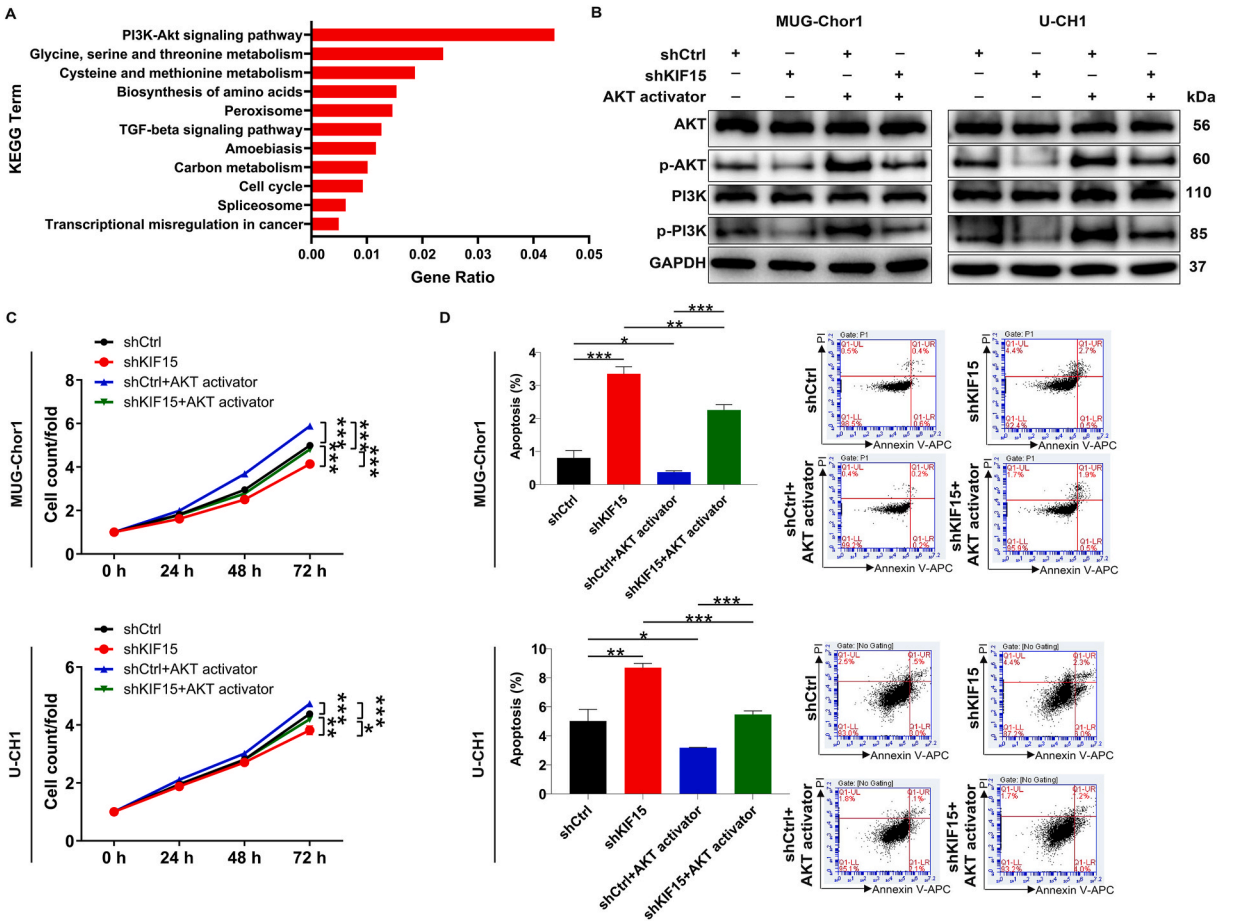

Fig. 5. KIF15 activates the PI3K-AKT pathway. (A) The signalling pathways related to KIF15 were obtained from KEGG analysis. (B) After being treated with 10 μM AKT activator, the total protein and phosphorylation levels of AKT and PI3K were evaluated in KIF15-silenced cells through Western blot. (C) After being treated with AKT activator, CCK8 assay showed the abilities to grow in KIF15-silenced MUG-Chor1 and U–CH1 cells. (D) Flow cytometry experiment detected cell apoptosis levels of KIF15-depleted MUG-Chor1 and U–CH1 cells following AKT activator addition. Results are presented as mean ± SD. $*P < 0.05$, $**P < 0.01$, $***P < 0.001$.

in MUG-Chor1 and U–CH1 cells significantly hampered cell proliferation ($P < 0.001$, Fig. 2A). Moreover, wound healing assays demonstrated a notable decrease in cell migration rates, with MUG-Chor1 cells exhibiting a 48 % decrease ($P < 0.01$) and U–CH1 cells demonstrating a 73 % reduction ($P < 0.001$) (Fig. 2B). These findings were consistent with results from Transwell assays ($P < 0.001$, 73 % for MUG-Chor1 cells and 99 % for U–CH1 cells; Fig. 2C). Flow cytometry analysis revealed that KIF15 depletion significantly elevated apoptosis in both MUG-Chor1 and U–CH1 cells (Fig. 3A; $P < 0.01$). Additionally, there was an increase in the percentage of cells in the G2 phase following shKIF15 transfection in both cell lines (Fig. 3B). To delve deeper into KIF15's functional role, we treated MUG-Chor1 and U–CH1 cells with 10 μM GW406108X, a KIF15 inhibitor. Subsequent assessments showed a significant inhibition of cell proliferation and an increase in apoptosis in the KIF15 inhibitor group compared to the control group (Fig. 3C and D). Overall, these results underscored that silencing KIF15 not only impedes cell proliferation and migration but also triggers apoptosis, leading to G2 phase cell cycle arrest.

3.4. Silencing KIF15 impairs chordoma tumour growth in vivo

We investigated the impact of KIF15 knockdown on tumour growth *in vivo* using xenograft models established in nude mice by injecting shCtrl- or shKIF15-transfected MUG-Chor1 cells subcutaneously (Fig. 4A). Reduced fluorescence in the shKIF15 group indicated inhibited tumour growth ($P < 0.01$, Fig. 4B). Additionally, assessment of tumour parameters, including weight and size, confirmed suppressed tumour growth in the shKIF15 group ($P < 0.05$, Fig. 4C–E). Furthermore, tumour tissues from the shKIF15 group showed a decreased Ki-67 index compared to the shCtrl group (Fig. 4F). These results collectively demonstrate that KIF15 knockdown leads to impaired tumorigenicity of chordoma cells *in vivo*, consistent with our *in vitro* findings.

3.5. KIF15 activates the PI3K-AKT pathway

To decipher the regulatory role of KIF15 in chordoma, we performed Kyoto Encyclopedia of Genes and Genomes (KEGG) pathway analysis on upregulated genes associated with elevated KIF15 levels, identified through a PrimeView human gene expression array. The analysis highlighted significant enrichment in various biological pathways, notably the PI3K-AKT signalling pathway (Fig. 5A). To delve deeper into this discovery, we treated KIF15-silenced MUG-Chor1 and U–CH1 cells with a 10 μM AKT activator. The results indicated that the decreased levels of *p*-AKT and p-PI3K in KIF15-depleted cells were restored upon AKT activator addition (Fig. 5B and S1D). Additionally, we found that the suppressed cell proliferation resulting from KIF15 downregulation was reversed with AKT activator treatment (Fig. 5C). Simultaneously, the heightened apoptosis levels in KIF15-silenced cells were alleviated following exposure to the AKT activator (Fig. 5D). Conversely, we engineered KIF15-overexpressing chordoma cells and exposed them to a 40 μM LY294002 (PI3K inhibitor). Firstly, we validated the efficacy of KIF15 overexpression in MUG-Chor1 and U–CH1 cells using Western blot analysis (Figure S2A). Subsequent Western blot assays unveiled the upregulation of *p*-AKT and p-PI3K in KIF15-overexpressed chordoma cells, which was reversed upon LY294002 addition (Figure S2B). Assessment of cell phenotypes in KIF15-overexpressed cells revealed that LY294002 elicited contrasting effects, including attenuated proliferation and augmented apoptosis (Figure S2C and S2D. Consequently, we conclude that KIF15 promotes chordoma development by activating the PI3K-AKT signalling pathway.

4. Discussion

Chordomas, rare and malignant tumours primarily affecting vertebral bones, are known for their local aggressiveness and high recurrence rates [1,2]. Traditional radiotherapy and chemotherapy have proven ineffective against chordoma tumours, making surgery the preferred treatment modality [5]. Despite surgical interventions, postoperative recurrence remains a common challenge, with a dismal prognosis observed in up to 40 % of chordoma cases [19,20]. In recent decades, the advent of molecular targeted therapy has provided new hope for individuals affected by chordomas. The distinct advantage of targeted therapy lies in its ability to selectively inhibit specific molecules or signalling pathways, thereby suppressing tumour growth and promoting apoptosis in tumour cells [21]. Receptor tyrosine kinase inhibitors like Imatinib, Nilotinib, and Sunitinib have shown promise by targeting platelet-derived growth factor receptors-α and β [22]. Furthermore, research into key molecular players such as P53 [23], PTEN [24], CDKN2A/2B [25], and MGMT [26] sheds light on chordoma development, suggesting potential therapeutic targets. In this context, we explored the role of KIF15 in chordoma progression, proposing it as a promising therapeutic target for chordoma treatment.

KIF15, a microtubule-dependent motor protein also known as kinesin-12, plays a critical role in bipolar spindle assembly and mitosis [12]. It has been recognized as a regulator of axonal development and contributes to maintaining spindle bipolarity during cellular processes [27]. Research by Liu et al. suggests that KIF15 is highly expressed in the cortex and ganglia during embryonic stages, with a gradual decline as neurons mature [28]. Previous studies have explored KIF15's role in various human cancers. In breast cancer, it's implicated in cell proliferation, migration, and cell cycle regulation due to its overexpression [17]. Similarly, elevated levels of KIF15 are associated with a poorer prognosis in lung adenocarcinoma patients [29]. Wang et al. demonstrated that KIF15 promotes pancreatic cancer cell proliferation by modulating the MEK/ERK pathway [15]. Remarkably, despite these findings, the potential of KIF15 as a therapeutic target for chordomas has not been previously investigated and warrants further exploration.

In the present study, we observed elevated levels of KIF15 expression in late-stage chordoma tissues. Subsequent *in vitro* experiments demonstrated that knockdown of KIF15 significantly impacted various chordoma cell behaviors, including reduced proliferation, increased apoptosis, and G2 phase arrest. This effect was consistent with the suppression of tumour growth observed in *in vivo* mouse xenograft models following KIF15 knockdown. Although one mouse in the shCtrl group exhibited delayed tumour formation compared to the others, we included this data to accurately represent experimental conditions and acknowledge inherent biological

variability. Notably, while no significant differences were observed in cell proliferation between 24 h and 48 h, a substantial discrepancy was noted in cell migration after 24 h. These findings suggest that KIF15 may play a more prominent role in regulating cell migration rather than proliferation at specific time points, reflecting its involvement in microtubule dynamics crucial for cell structure and movement [30,31]. Moreover, the temporal dynamics of cellular responses to KIF15 knockdown may vary, with migration-related processes showing earlier and more pronounced effects than proliferation. This nuanced understanding highlights the multifaceted roles of KIF15 in cellular behaviors.

Our investigation into KIF15-regulated chordoma mechanisms found that genes upregulated by KIF15 overexpression mainly clustered in the PI3K-AKT pathway, consistent with a previous study linking KIF15 with AKT. For example, Wang et al. demonstrate high KIF15 levels in gallbladder cancer development, where KIF15 knockdown suppressed cancer progression by reducing activity in several pathways, including PI3K/AKT [32]. Treating shCtrl- and shKIF15-transfected cells with an AKT activator showed that KIF15 deficiency's anti-tumour effects were lessened, while elevated KIF15 levels' pro-tumour effects were reversed with LY294002 treatment. These results suggest the active involvement of the PI3K-AKT pathway in KIF15-induced chordoma.

The PI3K-AKT pathway plays a crucial role in normal cellular functions and is often dysregulated in various malignancies, including chordomas, impacting processes, such as autophagy [33], epithelial-mesenchymal transition (EMT) [34], and apoptosis [35]. Studies, like Otani et al., have linked PI3K/AKT activation with brachyury overexpression, a key factor in chordoma growth [36]. Additionally, miR-31-5p has been found to protect against chordoma by activating the PI3K-AKT pathway [37]. Collectively, these findings underscore the pathway's intricate involvement in chordoma progression, offering potential therapeutic targets.

Acknowledging our study's reliance on cell lines to explore the PI3K-AKT pathway's role in chordoma, we recognize the need for *in vivo* validation. Furthermore, the specific regulatory mechanisms, notably how KIF15 influences the PI3K-AKT pathway, remain unexplored in our current work. To address these gaps, future plans include comprehensive *in vivo* experiments to validate the pathway's role in chordoma and further investigate KIF15's mechanisms in regulating chordomas.

5. Conclusions

In summary, our findings suggest that KIF15 promotes chordoma tumour progression by stimulating the PI3K-AKT signalling pathway. This highlights KIF15 as a potential therapeutic target for future interventions.

Ethics statement

The research was approved by the Medical Ethics committee of Guangdong Provincial People's Hospital (20203357035). The animal experiments adhered to the European Parliament Directive (2010/63/EU).

CRediT authorship contribution statement

Jinxing Yang: Writing – review & editing, Writing – original draft, Conceptualization. **Lijun Liu:** Software, Formal analysis, Data curation. **Xu Xu:** Validation, Software, Formal analysis. **Hui Zeng:** Writing – review & editing.

Declaration of competing interest

The authors declare that they have no known competing financial interests or personal relationships that could have appeared to influence the work reported in this paper.

Acknowledgement

Not applicable.

Appendix A. Supplementary data

Supplementary data to this article can be found online at https://doi.org/10.1016/j.heliyon.2024.e29386.

References

[1] Y. Yakkioui, J.J. Van Overbeeke, R. Santegoeds, M. Van Engeland, Y. Temel, Chordoma: the entity, BBA - Reviews on Cancer 1846 (2) (2014) 655–669.
[2] N.R. Smoll, O.P. Gautschi, I. Radovanovic, K. Schaller, D.C. Weber, Incidence and relative survival of chordomas, Cancer 119 (11) (2013) 2029–2037.
[3] V. Ulici, J. Hart, Chordoma, Arch. Pathol. Lab Med. 146 (3) (2022) 386–395.
[4] G.Y. Hung, J.L. Horng, H.J. Yen, C.C. Yen, W.M. Chen, C.H. Chen, et al., Incidence patterns of primary bone cancer in taiwan (2003–2010): a population-based study, Ann. Surg Oncol. 21 (8) (2014) 2490–2498.
[5] J. Lee, N.N. Bhatia, H.H. Bang, A. Ziogas, J.A. Zell, Analysis of prognostic factors for patients with chordoma with use of the California cancer registry, J. Bone Jt. Surg. Am. Vol. 94 (4) (2012) 356–363.
[6] S. Crunkhorn, Targeted therapy for chordoma, Nat. Rev. Drug Discov. 18 (3) (2019) 174.

[7] O.O. Akinduro, P. Suarez-Meade, D. Garcia, D.A. Brown, R. Sarabia-Estrada, S. Attia, et al., Targeted therapy for chordoma: key molecular signaling pathways and the role of multimodal therapy, Target Oncol 16 (3) (2021) 325–337.
[8] S. Stacchiotti, A. Longhi, V. Ferraresi, G. Grignani, A. Comandone, R. Stupp, et al., Phase II study of imatinib in advanced chordoma, J. Clin. Oncol. (2012).
[9] K. Chen, J. Mo, M. Zhou, G. Wang, G. Wu, H. Chen, et al., Expression of PTEN and mTOR in sacral chordoma and association with poor prognosis, Med. Oncol. 31 (4) (2014) 886.
[10] I.M. Siu, J. Ruzevick, Q. Zhao, N. Connis, Y. Jiao, C. Bettegowda, et al., Erlotinib inhibits growth of a patient-derived chordoma xenograft, PLoS One 8 (2013).
[11] K. Yohei, S. Hikaru, K. Tokuhiro, M. Tomoru, T. Satoshi, K. Takeshi, et al., Molecular and clinical risk factors for recurrence of skull base chordomas: gain on chromosome 2p, expression of brachyury, and lack of irradiation negatively correlate with patient prognosis, J. Neuropathol. Exp. Neurol. (9) (2013) 816.
[12] E.G. Sturgill, S.R. Norris, Y. Guo, R. Ohi, Kinesin-5 inhibitor resistance is driven by kinesin-12, JCB (J. Cell Biol.) 213 (2) (2016) 213–227.
[13] Peter Tatrai, Gayathri Chandrasekaran, Fanni Gergely, Hitting the brakes: targeting microtubule motors in cancer, Br. J. Cancer (2015).
[14] L. Gao, W. Zhang, J. Zhang, J. Liu, F. Sun, H. Liu, et al., KIF15-Mediated stabilization of AR and AR-V7 contributes to enzalutamide resistance in prostate cancer, Cancer Res. 81 (4) (2021) 1026–1039.
[15] J. Wang, X. Guo, C. Xie, J. Jiang, KIF15 promotes pancreatic cancer proliferation via the MEK-ERK signalling pathway, Br. J. Cancer (2017).
[16] H. Zhao, Q. Bo, Z. Wu, Q. Liu, Y. Li, N. Zhang, et al., KIF15 promotes bladder cancer proliferation via the MEK–ERK signaling pathway, Cancer Manag. Res. 11 (2019) 1857–1868.
[17] X. Gao, L. Zhu, X. Lu, Y. Wang, G. Jiang, KIF15 contributes to cell proliferation and migration in breast cancer, Hum. Cell (6) (2020).
[18] B. Milic, A. Chakraborty, K. Han, M.C. Bassik, S.M. Block, KIF15 nanomechanics and kinesin inhibitors, with implications for cancer chemotherapeutics, Proc Natl Acad U S A (2018).
[19] Z. Wu, J. Zhang, L. Zhang, G. Jia, J. Tang, L. Wang, et al., Prognostic factors for long-term outcome of patients with surgical resection of skull base chordomas-106 cases review in one institution, Neurosurg. Rev. 33 (4) (2010) 451.
[20] R.J. Diaz, N. Maggacis, S. Zhang, M.D. Cusimano, Determinants of quality of life in patients with skull base chordoma, J. Neurosurg. 120 (2) (2014) 528–537.
[21] C. Palena, D.H. Hamilton, R.I. Fernando, An immunotherapeutic intervention against tumor progression: targeting a driver of the epithelial-to-mesenchymal transition, OncoImmunology (2014).
[22] Q.I. Nan, D.U. Nan, X. Wei, B.Y. Chen, L.I. Xiao-Song, M.A. Jun-Xun, et al., A clinical study of imatinib in the treatment of advanced chordoma patients, Chinese Journal of Bone & Joint (2014).
[23] Y. Ma, B. Zhu, X. Liu, Z. Liu, G. He, iASPP overexpression is associated with clinical outcome in spinal chordoma and influences cellular proliferation, invasion, and sensitivity to cisplatin in vitro, Oncotarget 8 (40) (2017) 68365–68380.
[24] Lee Dae-Hee, Zhang Ying, Kassam Amin, et al., Combined PDGFR and HDAC inhibition overcomes PTEN disruption in chordoma, PLoS One (2015).
[25] Y. Tsutsumi, Y. Chinen, N. Sakamoto, H. Nagoshi, K. Nishida, S. Kobayashi, et al., Deletion or methylation of CDKN2A/2B and PVT1 rearrangement occur frequently in highly aggressive B-cell lymphomas harboring 8q24 abnormality, Leuk. Lymphoma (2013).
[26] G. Marucci, L. Morandi, D. Mazzatenta, G. Frank, E. Pasquini, M.P. Foschini, MGMT promoter methylation status in clival chordoma, Journal of neuro-oncology 118 (2) (2014) 271–276.
[27] Z. Dong, S. Wu, C. Zhu, X. Wang, Y. Li, X. Chen, et al., Clustered Regularly Interspaced Short Palindromic Repeats (CRISPR)/Cas9-mediated kif15 mutations accelerate axonal outgrowth during neuronal development and regeneration in zebrafish, Traffic 20 (1) (2019) 71.
[28] Z. Dong, S. Wu, C. Zhu, X. Wang, Y. Li, X. Chen, et al., CRISPR/Cas9-.-ediated kif15 mutations accelerate axonal outgrowth during neuronal development and regeneration in zebrafish, Traffic 20 (2018).
[29] G. Bidkhori, Z. Narimani, S.H. Ashtiani, A. Moeini, A. Nowzari-Dalini, A. Masoudi-Nejad, Reconstruction of an integrated genome-scale Co-expression network reveals key modules involved in lung adenocarcinoma, PLoS One (2013).
[30] L. Wordeman, How kinesin motor proteins drive mitotic spindle function: lessons from molecular assays, Semin. Cell Dev. Biol. 21 (3) (2010) 260–268.
[31] B.J. Mann, S.K. Balchand, P. Wadsworth, Regulation of Kif15 localization and motility by the C-terminus of TPX2 and microtubule dynamics, Mol. Biol. Cell 28 (1) (2017) 65–75.
[32] J. Wang, D. Wang, Z. Fei, D. Feng, B. Zhang, P. Gao, et al., KIF15 knockdown suppresses gallbladder cancer development, Eur. J. Cell Biol. 100 (7–8) (2021) 151182.
[33] Z. Xu, X. Han, D. Ou, T. Liu, Z. Li, G. Jiang, et al., Targeting PI3K/AKT/mTOR-mediated autophagy for tumor therapy, Appl. Microbiol. Biotechnol. 104 (2) (2020) 575–587.
[34] W. Xu, Z. Yang, N. Lu, A new role for the PI3K/Akt signaling pathway in the epithelial-mesenchymal transition, Cell Adh Migr 9 (4) (2015) 317–324.
[35] X. Jia, Z. Wen, Q. Sun, X. Zhao, H. Yang, X. Shi, et al., Apatinib suppresses the proliferation and apoptosis of gastric cancer cells via the PI3K/akt signaling pathway, J BUON 24 (5) (2019) 1985–1991.
[36] R. Otani, A. Mukasa, M. Shin, M. Omata, S. Takayanagi, S. Tanaka, et al., Brachyury gene copy number gain and activation of the PI3K/Akt pathway: association with upregulation of oncogenic Brachyury expression in skull base chordoma, J. Neurosurg. 128 (5) (2018) 1428–1437.
[37] W. Wang, L. Tang, Q. Li, J. Tan, H. Yao, Z. Duan, et al., Overexpression of miR-31-5p inhibits human chordoma cells proliferation and invasion by targeting the oncogene c-Met through suppression of AKT/PI3K signaling pathway, Int. J. Clin. Exp. Pathol. 10 (7) (2017) 8000–8009.